Design, synthesis and evaluation of novel pyrimidinylaminothiophene derivatives as FGFR1 inhibitors against human glioblastoma multiforme

Yong-Liang Li, Long-Jia Yan, Hui-Xiong Chen, Ban-Kang Ruan, Pascal Dao, Zhi-Yun Du, Chang-Zhi Dong, Bernard Meunier

Version of Record: https://www.sciencedirect.com/science/article/pii/S0223523423007316
Manuscript_bd87e65c791ccf099c629870dc071645

Design, synthesis and evaluation of novel pyrimidinylaminothiophene derivatives as FGFR1 inhibitors against human glioblastoma multiforme

Yong-Liang Li[1,†], Long-Jia Yan[1,†], Hui-Xiong Chen[1,2,*], Ban-Kang Ruan[1], Pascal Dao[3], Zhi-Yun Du[1,*], Chang-Zhi Dong[1,4], Bernard Meunier[1,5]

[1]School of Chemical Engineering and Light Industry, Guangdong University of Technology, Guangzhou, P. R. China

[2]Chemistry of RNA, nucleosides, peptides and heterocycles, CNRS UMR8601, Université Paris Cité, UFR Biomédicale, 45 rue des Saints-Pères, 75270 Paris Cedex 06, France

[3]Université Côte d'Azur, CNRS, Institut de Chimie de Nice UMR7272, Nice, France

[4]Université Paris Cité, ITODYS, UMR 7086 CNRS, 75013 Paris, France

[5]Laboratoire de Chimie de Coordination du CNRS, 205 Route de Narbonne, 31077 Toulouse Cedex, France.

*Correspondence: huixiong.chen@parisdescartes.fr; zhiyundu@foxmail.com

[†]Yong-Liang Li and Long-Jia Yan contributed equally to this work

Abstract

Vascular endothelial growth factor receptors (VEGFRs) have emerged as the most promising anti-angiogenic therapeutic targets for the treatment of recurrent glioblastomas (GBM). However, anti-VEGF treatments led to the high proportion of non-responder patients or non lasting clinical response and the tumor progression to the greater malignant stage. To overcome these problems, there is an utmost need to develop innovative anti-angiogenic therapies. In this study, we report the development of a series of new FGFR1 inhibitors. Among them, compound **4i** was able to potently inhibit FGFR1 kinase activities both *in vitro* and *in vivo*. This compound displayed strong anti-angiogenic activity in HUVECs and anti-tumor growth and anti-invasion effects in U-87MG cell line. These results emphasize the

importance of FGFR1-mediated signaling pathways in GBM and reveal that pharmacological inhibition of FGFR1 can enhance the anti-tumoral, anti-angiogenic and anti-metastatic efficiency against GBM. These data support targeting of FGFR1 as a novel anti-angiogenic strategy and highlight the potential of compound **4i** as a promising anti-angiogenic and anti-metastatic candidate for GBM therapy.

Keywords : FGFR1, Inhibitor, Anti-angiogenesis, Metastasis, Glioblastomas

1. Introduction

Glioblastoma, also known as glioblastoma multiforme (GBM), is the most infiltrative, aggressive and highly vascularized brain tumor, which can occur at any age, but more often in older adults. Currently available treatment options including surgery, chemotherapy and radiation for patients with GBM have limited efficacy and the median survival time is only 15 to 16 months in people who get these treatments [1]. There is therefore an utmost need to develop innovative targeted therapies because of poor clinical outcome for the treatement of glioblastoma patients.

Anti-angiogenesis therapy is one of the most effective cancer treatments. Tumor angiogenesis, where new turmor vessels sprout from existing vasculature in place is a complex multistep procedure, which is controled by a balance between various pro and anti-angiogenic factors and their receptors [2]. The well-characterized pro-angiogenic factors and signaling pathways implicated in tumor angiogenesis are vascular endothelial growth factor receptors (VEGFRs), which have emerged as the most promising anti-angiogenic therapeutic targets in most solid cancers [3]. Since the first anti-angiogenic drug Avastin, a milestone in cancer research and therapy was approved by FDA in 2004, a number of drug targeting VEGF ligands or their receptors (VEGFRs) have been successfully developed and provided as new ammunition against cancer. FDA has also authorized a monoclonal antibody, Bevacizumab as anti-angiogenic drug to treat recurrent GBM, which binds to VEGF, disrupts new blood vessel formation and increases progression-free survival [4]. Furthermore, a number of VEGFR tyrosine kinase inhibitors have also demonstrated significant anti-angiogenic and anti-tumor activity in mouse models of GBM and in phase I/II clinical trials [5,6]. However, anti-VEGF treatments resulted in the high proportion of non-responder patients or non lasting clinical response due to the intrinsic or acquired resistance [7]. The underlying mechanisms of resistance to anti-VEGFR agents among patients with GBM remain unclear, although several types of resistance to anti-angiogenic therapy such as adaptive or evasive resistance and intrinsic non-responsiveness have been described [8]. Moreover, it is also observed that angiogenesis inhibitors targeting the VEGF pathway resulted in the tumor progression to the greater malignant stage due to

heightened invasion into surrounding tissue and increase of lymphatic and distant metastasis [9].

Tumor angiogenesis is a complex multistep process. In addition to VEGF/VEGFR, it also involves many other angiogenic factors and their receptors including Fibroblast growth factor receptor 1 (FGFR1), which is reported not only to play an important role in pathological angiogenesis, but also to contribute to tumorigenesis and metastasis in patients with different types of malignancies [10-12]. FGFR1 gene is located at the human chromosomal locus 8p12, which codes two FGFR1b and FGFR1c isoforms. When bound to a proper FGF, FGFR1 elicits cellular responses, which are related with many biological functions including cellular proliferation, survival, migration and angiogenesis. FGFR1 gene is often activated due to its duplication, point mutation and fusion with other genes such as Transforming acidic coiled-coil gene 1 (TACC1) and 3 (TACC3) [13,14]. The fusion gene products are constitutively active and able to transduce aberrant signals through FGFR1 signaling pathway. Aberrant activation of FGFR1 signaling is associated with growth, invasion and stemness in glioblastomas [15]. Moreover, an overexpression of FGFR1 is observed in high-grade gliomas, which is largely higher than that in normal brain [16] and associated with increased migration of glioma cells [17,18].

Great efforts have been devoted to inhibit FGFR-mediated signaling pathways as anti-cancer angiogenesis and anti-cancer growth therapy. The first generation of FDA-approved small-molecule targetting FGFR drugs are multi-target inhibitors, including Pazopanib [19], Regorafenib [20] and Lenvatinib [21] which exert anti-tumor efficacy (Fig. 1). A second generation of FDA-approved small-molecule inhibitors with greated selectivity for FGFR (Erdafitini, Infigratinib and Pemigatinib, Fig. 1) has been recently used in clinical practice to treat advanced/metastatic urothelial carcinoma and cholangiocarcinoma [22-24]. Although FGFR1 signaling pathways play significant roles in human glioblastoma angiogenesis, growth and invasion, there is no FGFR1 targetting therapy for the treatment of glioblastomas.

It is known that 2,4-diarylaminopyrimidine is a useful scaffold in the design of anti-cancer agents and FGFR inhibitors [25,26]. Therefore, we have developed a series

of new FGFR1 inhibitors with this fragment. These compounds with different docking scores (Table S1) were characterized based on their bond energy and binding capacity analysis [27]. Then, the validation of such structures was identified by an ADP-Glo^{TM} kinase assay, demonstrating a potent inhibition of FGFR1 activity with IC_{50} values in the 10^{-7}-10^{-8} M range. The best inhibitor of this series of compounds exhibited an IC_{50} value of 0.028±0.001 μM, which is consistent with the docking scoring rankings of compound **4i**. The bioactivities of the compound **4i** with therapeutic potential were subsequently evaluated both *in vitro* and *in vivo*. These results reveal that the inhibition of FGFR1 signaling pathways can enhance anti-tumoral, anti-angiogenic and anti-metastatic efficiency, providing the promissing potential to serve as a new alternative avenue for angiogenic therapy to treat glioblastomas.

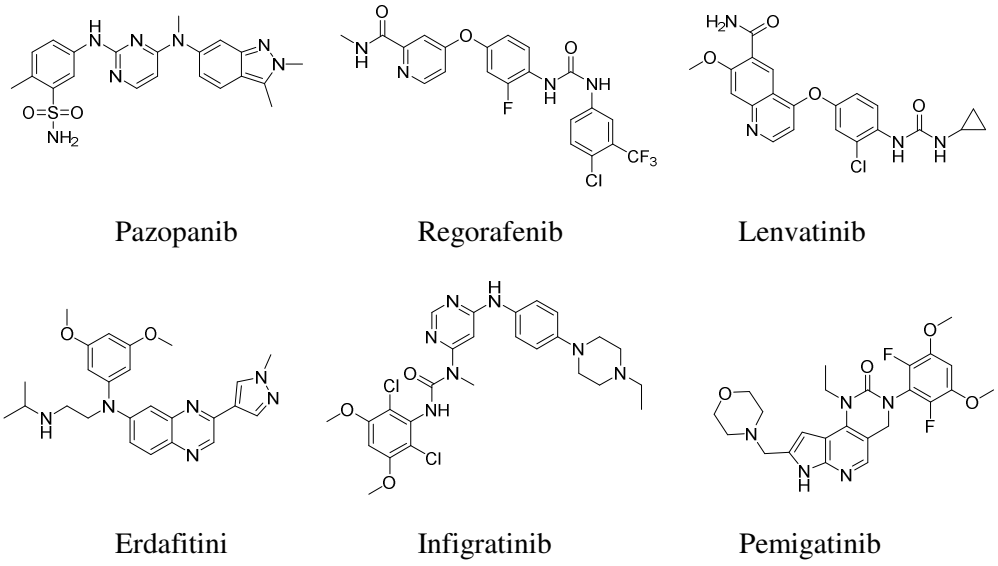

Fig. 1 Selected FDA-approved small-molecule FGFR inhibitors

2. Results and discussion

2.1. Chemistry

The synthetic route of target compounds **4** was shown in **Schemes 1** and **2**. Initially, 2-aminothiophene derivatives **1** was prepared by the Gewald reaction in 64-80% yield. 5-trifluoromethyl-2,4-dichloropyrimidine reacted with 4-morpholin-4-yl-phenylamine at the presence of $ZnCl_2$ to give intermediate **2a**

followed by a condensation with **1** in the presence of TFA as catalyse to obtain the target compounds **4a-d**. On the other hand, the compounds **4e-3p** were achieved by two nucleophilic substitutions of variously substituted 2,4-dichloropyrimidine with **1a** followed by the corresponding arylamine in 20.4–43.5% yields for two steps.

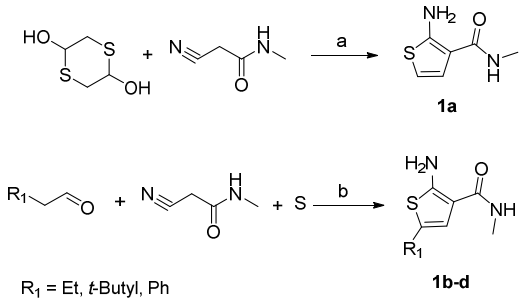

Scheme 1. Synthetic route for compounds **1**. Reagents and conditions: a) TEA, EtOH, reflux; b) TEA, EtOH, 45 °C.

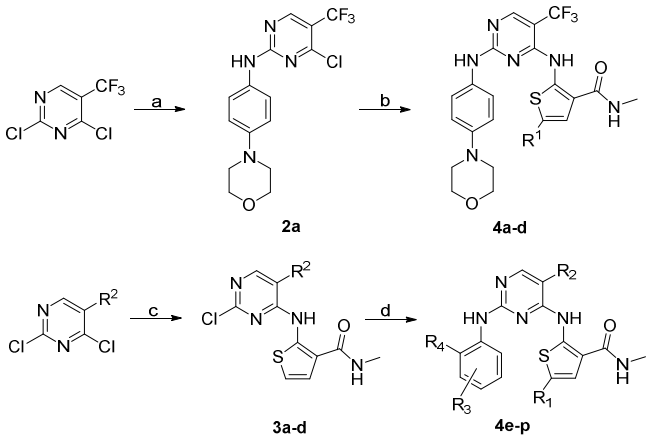

Scheme 2. Synthetic route for compounds **4**. Reagents and conditions: a) $ZnCl_2$, DCE, TEA, 0-5 °C; b) TEA, EtOH, 50 °C; c) $NaHCO_3$, EtOH, reflux; d) TFA, TFE, reflux.

2.2. Structure-activity relationships

The inhibitory activity of the synthesized new compounds **4** was first assayed for their activities against FGFR1 using an ADP-Glo^{TM} kinase assay. A known inhibitor of FGFR, AZD4547 [28] was included as a control in this assay.

As shown in Table 1, we first investigated the influence of the introduction of different groups R1 on the position 5 of the thiophene ring (compounds **4b**-**d**) and

found these compounds resulted in a large decrease in inhibitory potency on FGFR1 kinase activity, as compared to the corresponding compound **4a** (IC_{50} 0.061±0.004 μM). The displacement of the morpholine group from ortho (compound **4a**) to meta position in the arylamine on the ring B (compound **4e**) was not well tolerated and led to a decreased potency affinity toward FGFR1. Then, we investigated the replacement of morpholine moiety on the phenyl ring (ring B) by different groups leading to compounds **4f**-**l**. Among them, we noted that compounds **4f**-**h** displayed a significant improvement in inhibitory activity against FGFR1, especially for compound **4f** (IC_{50} 0.028±0.004 μM). It is interesting to note that further substitution on this compound by the introduction of a methoxy group at the position 2' of the phenyl ring (ring B) provide compound **4m**, which lost potency towards to FGFR1 kinase activity (IC_{50} 0.097±0.008 μM). Finally, replacing the trifluomethyl group (compound **4i**) with several groups such as methyl, chloro and bromo groups leading to compounds **4n–p** were well tolerated, except for compound **4p** and resulted in only a marginal loss in potency.

Then, the compounds **4** was further evaluated for their anti-proliferative effect on U-87MG cell line using the MTT assay (Table 1). Most of the tested compounds demonstrated good activities against U-87MG cell line at similar levels to those observed with their inhibitory potency on FGFR1 enzymatic activity, except for compounds **4a-c**, which have much lower potency on the U-87MG cell line, possibly due to their poor delivery and low bioavailability. It worth noting that compound **4i**, exhibited the higher anti-tumorigenic effects in U-87MG cells with IC_{50} values of 2.38 ± 0.31 μM, more potent than AZD4547 (25.41 ± 3.9 μM). Similar result was also observed *in vitro* colony formation to show the anti-tumorigenic effects with IC_{50} values of 0.12 ± 0.02 μM (data not shown). Furthermore, compound **4i** was evaluated against normal fibroblast NIH/3T3 cells and found to be relatively less toxic (data not shown). Based on the results above, we selected compound **4i** for further study due to its good potency in both enzymatic and anti-proliferative assays.

Table 1: *In vitro* enzymatic and cellular activities of new compounds **4** against FGFR1 compared with AZD4547

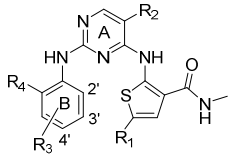

N°	R_1	R_2	R_3	R_4	FGFR1 IC_{50} (μM)	U-87MG IC_{50} (μM)
4a	H	CF_3	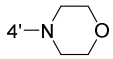	H	0.061±0.004	＞ 50
4b	Et	CF_3	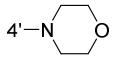	H	0.13±0.02	＞ 50
4c	t-Bu	CF_3	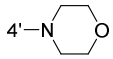	H	0.34±0.03	＞ 50
4d	Ph	CF_3	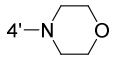	H	0.26±0.04	23.20±0.34
4e	H	CF_3	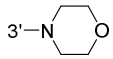	H	0.11±0.02	19.20±1.40
4f	H	CF_3	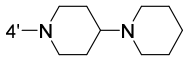	H	0.039±0.04	2.77±0.22
4g	H	CF_3	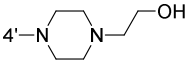	H	0.057±0.04	3.71±0.41
4h	H	CF_3	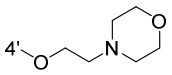	H	0.44±0.02	12.00±0.23
4i	H	CF_3	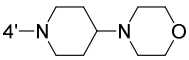	H	0.028±0.001	2.38±0.31
4j	H	CF_3	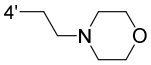	H	0.077±0.009	8.28±0.56
4k	H	CF_3	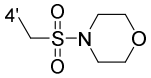	H	0.17±0.02	18.90±1.22
4l	H	CF_3	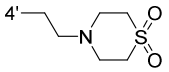	H	0.38±0.03	12.40±1.30
4m	H	CF_3	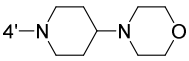	OCH_3	0.097±0.008	16.80±1.16
4n	H	Cl	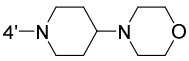	H	0.035±0.004	4.25±0.27
4o	H	Br	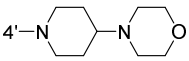	H	0.052±0.003	30.10±2.90
4p	H	CH_3	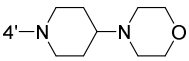	H	0.075±0.006	11.59±1.10
AZD4547					0.0011±0.0001	25.41±2.90

*2.3. Kinase inhibition profile and molecular docking of compound **4i***

The selectivity of compound **4i** was assessed *in vitro* against a panel of 20 kinases (Akt, Abl, BTK, c-kit, EGFR, ErbB2, Erk, FGFR1-4, VEGFR1-3, IGF-1R, MEK1/2, PDGFRα, c-Raf, Ros, mTOR), which was carried out with human recombinant proteins by Eurofins France (Paris), using radiometric kinase activity assays (Table S2). We noted that this compound only strongly inhibited FGFR1, showing a good selectivity profile against the other tested kinases.

In an attempt to better understand the putative binding mode of this inhibitor with FGFR1 kinases, compound **4i** was docked into the FGFR1 kinase structure (PDB ID: 6c1c). As shown in Fig. S1, compound **4i** fitted well into the ATP binding pocket of the kinases. We noted that 2,4-diarylaminosubstituted pyrimidine scaffold of compound **4i** adopted a line-shaped mode. The 2-aniline ring was sandwiched between residues Leu484 and Leu630, interacting with them via hydrophobic contacts. One NH of 2-aniline moiety was involved in a critical hydrogen bond with the CO of Ala564 on the hinge of the kinase, while another one of 4-thiophene moiety formed hydrogen bond with the CO of Lys566. An additional H-bond occurred between the nitrogen of pyrimidine nucleus and the amino group of Gly567. Moreover, the morpholine and piperidine rings occupied the hydrophobic pocket in the gate area, and interacted through hydrophobic interaction with the side chains of amino acids Met535, Ile545 and Val561.

*2.4. ADMET study and phamacokinetics of compound **4i** in rats*

Prior to the pharmacological research, we first determined ADMET descriptors to estimate the hepatotoxicity, absorption, solubility and blood-brain barrier (BBB) penetration and toxicity profile of compound **4i** by using Discovery Studio 2.5 software (Table S3-4, Fig. S2). ADMET CYP2D6 binding predicts compound **4i** is non-inhibitor of cytochrome P450 enzyme and the hepatotoxicity score is 0, expecting that compound **4i** is probably non hepatotoxic. Compound **4i**, classed as 0 for human intestinal absorption (HIA) has fallen inside 95% human intestinal absorption confidence ellipsoid, sugesting compound **4i** has good human intestinal absorption. In

addition, compound **4i** has fallen outside 99% BBB ellipse and cannot be defined. The toxicity profile was also investigated to show minimal toxicity prediction of compound **4i**. This compound was expected to be non-irritant for skin with moderate irritants for the eye. Rat oral LD_{50} of compound **4i** was predicted to be 1.01 g/kg. Taken together, it can be suggested that compound **4i** has desired properties to act as drugs.

Then, we evaluated the pharmacokinetic profiles of compound **4i** in rats. As shown in Fig. 2A, the plasma concentrations of compound **4i** following oral administration at 52.5 mg/kg apparently declined in a multi-exponential manner. The plasma concentration versus time profiles of this compound showed that a single dose of compound **4i** resulted in a peak concentration (Cmax) of 3.9 ± 0.5 μg/mL, a Tmax of 4.4 ± 2.6 h, a terminal half life ($t_{1/2}$) of 14.3 ± 1.7 h and an AUC of 71.5 ± 7.7 μg·h/mL (Table S5).

*2.5. Effect of compound **4i** on tumorigenesis in vivo in xenograft tumors*

We further studied the impact of compound **4i** on anti-cancer and anti-angiogenetic potential *in vivo* using U-87 MG xenograft models. Nude mice were subcutaneously implanted with U-87 MG cells and dosed orally 5 days/week for 4 weeks with 50 or 75 mg/kg per day. As shown in Fig. 2F, the tumor volumes of vehicle were increased to nearly 10 fold of starting volume from day 0 to day 28. However, they were clearly reduced in **4i**-treated mice. Indeed, the tumor volumes were only increased to less than 4-fold of starting volume with 50 mg/kg/d and even smaller than the starting volume with 75 mg/kg/d. After 4 weeks, the mice were euthanized and the tumors were taken out and weighted to further confirm that the mice injected with 75 mg/kg dose had lighter tumor weight than the mice injected with 50 mg/kg dose (Fig. 2H-I). These results demonstrated the potential therapeutic efficacy of compound **4i** for the treatment of human glioblastomas.

Moreover, we found that compound **4i** obviously decreased FGFR1 phosphorylation in tumor tissues (Fig. 2B-C). IHC staining showed that the expression of Ki67, a biomarker of proliferation, was remarkably inhibited with

compound **4i** treatment (Fig. 2J,L). In addition, cluster of differentiation 31 (CD31), an important marker of the small vessel endothelium to show the microvessel density was observed to be highly expressed in histological tumor tissue sections of the control (Fig. 2J,K). However, compound **4i** treatment strongly inhibited the expression of CD31. Indeed, **4i**-treated tumors with 50 mg/kg and 75 mg/kg showed 38.4 ± 1.3 % and 62.0 ± 0.9 % reduction in Ki67, compared with the vehicle control (Fig. 2L). Similarly, the proportion of CD31 positive expression was significantly decreased by 78.9 ± 5.2 % in **4i**-treated mice with 50 mg/kg and by 37.5 ± 3.7 % in **4i**-treated mice with 75 mg/kg, as compared with the vehicle control group (Fig. 2K). Furthermore, gelatinase-A (MMP-2) and gelatinase-B (MMP-9) belong to a family of the matrix metalloproteinases which are involved in tumor cell invasion angiogenesis and highly expressed in patients with WHO grade III brain tumors [29]. As illustrated in Fig. 2J, and 2M-N, the high expression of MMP-2 and MMP-9 was observed in the IHC staining and further confirmed by western blot analysis of the histological tumor tissue sections of the control. Conversely, excessive MMP-2/9 expressions were evidently attenuated after treatment with compound **4i**, especially for the MMP-9 expression.

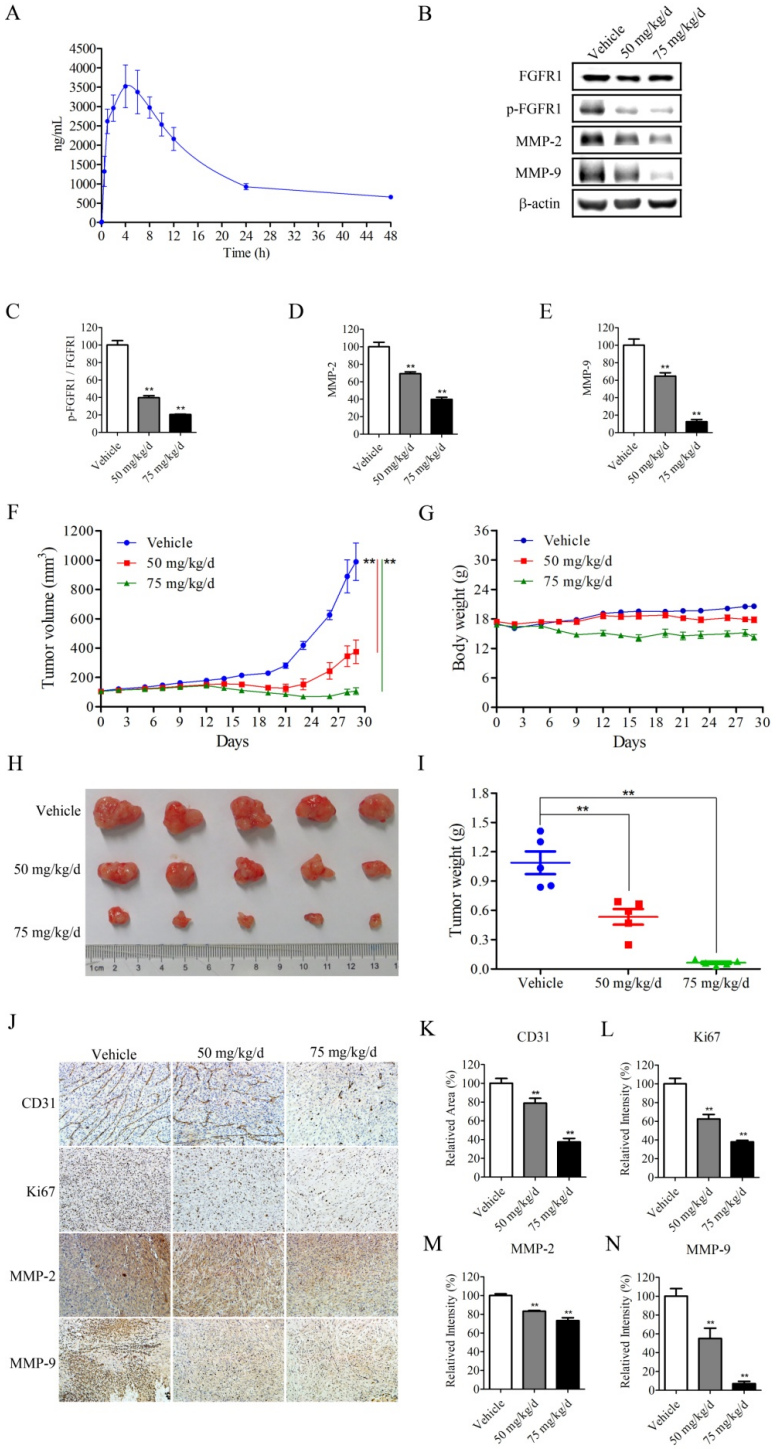

Fig. 2 Effect of compound **4i** on the U-87 MG human glioma cell growth *in vivo* via inhibition of angiogenesis. A) The plasma concentration of **4i** by oral administration 52.5 mg/kg in rat. B) The phosphorylation of FGFR1 and the expression levels of MMP-2/9 were examined by western blot in tumor tissue. C-E) The western blotting analysis. F) The tumor volume, the length of major axis (L) and minor axis (D) of tumors were recorded with vernier caliper and the tumor volume were calculated by (L× D2)/2. G) Body weight, the weight of

nude mice were recorded three times per week. H-I) Tumor weight of the mice at the end of the experiment. J-N) The expression levels of CD31, Ki67, MMP-2 and MMP-9 were determined by immunohistochemistry. Six images were collected from the random region (10 X), then the integral intensity of brown was calculated by using Image. Data were mean ± SD, **P*<0.05, ***P*<0.01 *vs.* DMSO group.

*2.6. Effect of compound **4i** on cell cycle and FGFR1-mediated signal pathways in U-87 MG cell line*

The anti-proliferative effect of compound **4i** on U-87 MG cell line was further investigated by quantifying the cell cycle phase distribution. U-87 MG cells were first treated with compound **4i** for 48 h and then stained with iropidium iodide (PI) to analyze the DNA content in each cell using flow cytometer. We noted that compound **4i** induced U-87 MG cell cycle arrest in the G2/M phase compared with the vehicle control (DMSO) (Fig. 3A), suggesting that compound **4i** exerts anti-proliferative effects on U-87 MG cells through the induction of cell cycle arrest in the G2/M phase. Indeed, for the cells treated with DMSO, cell cycle analysis of the population indicated the following distribution: G0/G1 and G2/M were 71.6 ± 6.3% and 14.5 ± 1.2%, respectively. Conversely, it was observed for the cells treated with compound **4i** at lower concentration (0.3 μM) that the cell population in the G2/M phase increased obviously from 14.5 ± 1.2% to 56.8 ± 4.7%, while the cell population in the G0/G1 phase reduced from 71.6 ± 6.3% to 34.4 ± 2.5%. Stronger effects were observed if U-87 MG cells were treated with higher concentrations of compound **4i** (1 and 3 μM).

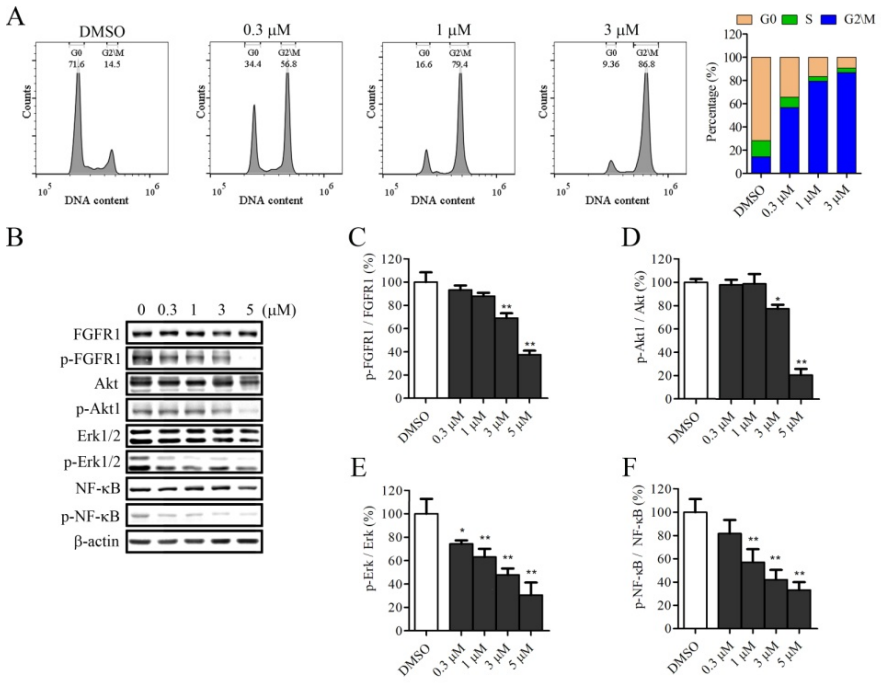

Fig. 3 Compound **4i** induces G2 cell cycle arrest in U-87 MG cell line. A) U-87 MG were treated with DMSO, **4i** at 0.3, 1 and 3 μM for 48 h. Cells were stained with PI and treated with RNase for 20 min. B) The phosphorylation of FGFR1 and its downstream, including p-Akt1, p-Erk1/2 and p-NF-κB were determined by western blotting. C-F) The western blotting analysis. Data were mean ± SD, n=3. **P* < 0.05, ***P* < 0.01 vs. DMSO group.

To further elucidate the mechanism by which compound **4i** inhibit U-87 MG cellular proliferation, we evaluated **4i**-mediated signaling proteins of FGFR1 in U-87 MG cells by western blot analysis. As shown in Fig. 3B-F, treatment of U-87 MG cells with compound **4i** reduced the phosphorylation of FGFR1, thereby resulting in the concomitant dose-dependent decrease of Akt, Erk and NF-κB phosphorylation levels. Indeed, untreated U-87 MG cell line revealed stronger positive immunostaining for activated diffuse cytoplasmic and scattered nuclear NF-κB, Akt and Erk phosphorylation, and a significant correlation of the phosphorylation levels was observed among p-654 FGFR1, p-Akt p-Erk and p-NF-κB. Of note, there was almost no direct effect of this compound on Akt and Erk activity.

*2.7. Compound **4i** decreases U87 cell adhesion, migration and invasion in a*

dose-dependent manner

Invasion and metastasis are the hallmark of cancer, which are responsible for 90% of all cancer deaths. Invasion is a process by which cancer cells penetrate into neighbouring or surrounding tissues. Metastasis is a process by which cancer cells spread into tissues and organs at a different location beyond the original place. Both processes facilitate the spreading of cancer cells into new tissues, which need to modify the interaction of cancer cells with extracellular matrix (ECM) ligands and to hydrolyze a range of ECM proteins so that they can leave their primary site [30]. Matrix metalloproteinases (MMPs), a family of metalloproteinases are able to degrade all kinds of ECM and play a key role in cell behaviors such as cell proliferation, migration, angiogenesis and host defense. Among them, MMP-2 and MMP-9 are correlated closely with the invasive properties of high grade gliomas both *in vitro* and *in vivo* [31]. The suppression of MMP-2 activity by antisense oligonucleotides also led to the loss of angiogenic potential, limited tumor vascularization and inhibited tumor growth [32]. GBM cells are primarily adherent to adjacent cells and ECM. GBM invasion escape surgery and led to a great obstacle for curative therapy [33].

We first determined the inhibitory effect on U-87 MG cell migration by Compound **4i**, using a scratch assay. As shown in Fig. 4A-B, compound **4i** had a negative impact on cell mobility with the reduced rate of cell migration to the scratched defect. Indeed, after creating a new artificial gap on the confluent U-87 MG cell monolayer, the scratched area were occupied by the migrated cells after 24 hours of incubation if they were treated with DMSO, whereas **4i**-treated cells moved more slowly and failed to close the artificialy created gap, especially at 5 μM.

Transwell assay is usually applied in studying the cell invasion ability. In this assay, U-87 MG cells were seeded on matrigel-coated well plates and treated with different doses of compound **4i** (0.3 or 3 μM) for 24 h. Under the microscope, we found U-87 MG cells passed through the matrigel-coated membrane and attached underneath of the upper chamber (Fig. 4C, E). In each microscope field (10X), the average number of cells treated with 0.1 % DMSO was 110 cells for 6 fields. However, the number of cells treated with compound **4i** at 0.3 or 3 μM under the

upper well were decreased to 71 and 24 for compound **4i**, suggesting that compound **4i** could reduce the invasion of U-87 MG cells, which correlated well with the *in vivo* studies.

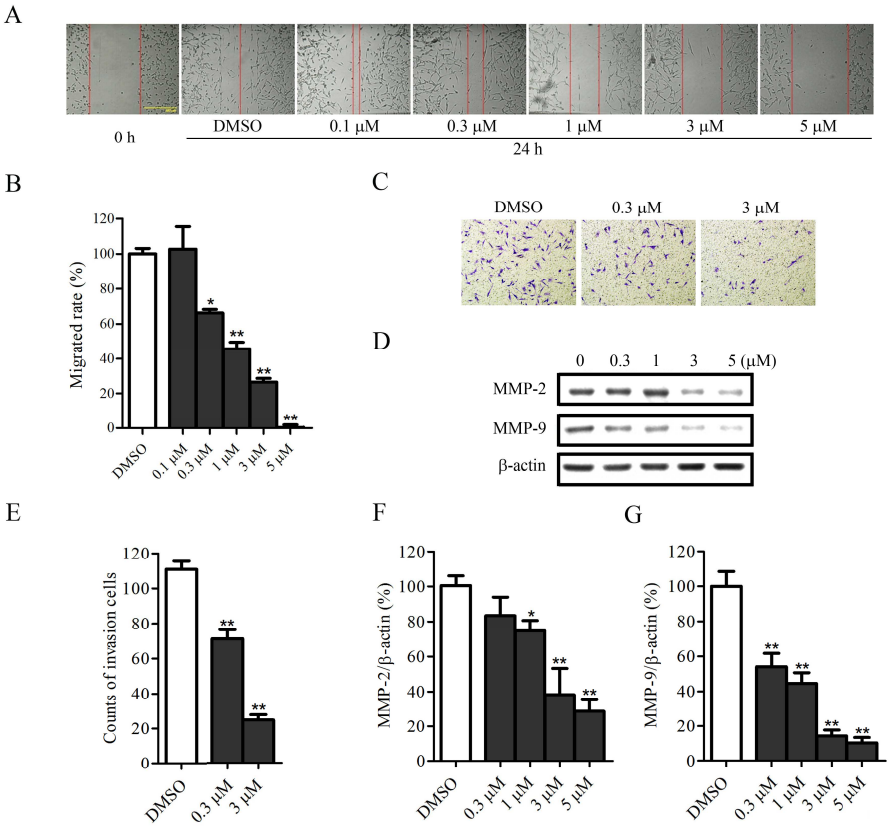

Fig. 4 Compound **4i** decreases U-87 MG cell adhesion, migration and invasion in U-87 MG cell line *in vitro*. A-B) The migration by wound healing assay in U-87 MG treated with DMSO, GD-CY484 at 0.1, 0.3, 1, 3 and 5 μM respectively for 24 h. Scale bar: 500 μm. C, E) The transwell invasion assay in U-87 MG treated with DMSO, **4i** at 0.3 and 3 μM respectively for 24 h and stained with crystal violet by transwell coated with matragel *in vitro* (10 X). D,F,G) The expression level of MMP-2 and MMP-9 in U-87 MG treated with **4i** at 0, 0.3, 1, 3 or 5 μM respectively. Data were mean ± SD, n=3. **P*<0.05, ***P*<0.01 *vs.* DMSO group.

It is known that matrix metalloproteinases 2 (MMP-2) and 9 (MMP-9) produced by tumor or stromal cells are the key factors involved in tumor migration, invasion and tumor-induced angiogenesis, and the suppression of their protein expression

could inhibit the cancer cell migration and invasion [29]. As shown in Fig. 4D, we detected the expression of MMP-2 and MMP-9 by using western blot method. Both of MMP-2 and MMP-9 expression were clearly decreased in U-87 MG cells treated with compound **4i** in a dose dependent manner, especially for the inhibition of MMP-9 expression, which is consistent with the results observed in **4i**-treated U87 migration and invasion as well as the *in vivo* studies.

*2.8. Effects of Compound **4i** on FGFR1 phosphorylation, cell adhesion and tube formation in HUVECs*

Endothelial cell proliferation, adhesion and tube formation are essential in the process of tumor angiogenesis. In this study, HUVEC cell line was chosen to assess the anti-angiogenic potential of compound **4i**.

We first determined whether compound **4i** could affect FGFR1 phosphorylation in HUVECs. As shown in Fig. 5A-B, when cells were treated in absence or in presence of compound **4i** at various concentrations for 48 h, Y654-FGFR1 phosphorylation was decreased in a concentration-dependent manner. Then, we evaluated *in vitro* the effect of compound **4i** on cell adhesion by exposing HUVECs to either various concentrations of inhibitor or DMSO vehicle control. Compound **4i** significantly inhibited the cell adhesion in a dose dependent-manner (Fig. 5C). In addition, tube formation of HUVEC cells was performed in absence or in presence of compound **4i** at 0.1 or 0.5 or 2 μM for 24 h and the endothelial tubes in three independent random samples were examined using light microscope in high magnification field. As shown in Fig. 5D-E, compound **4i** displayed a potent inhibitory activity against capillary tube formation, which consistent with the *in vivo* studies. Indeed, compound **4i** at 0.1, 0.5 and 2 μM inhibited capillary tube formation by 10.4 ± 4.9%, 59.7 ± 5.1% and 81.0 ± 3.0%.

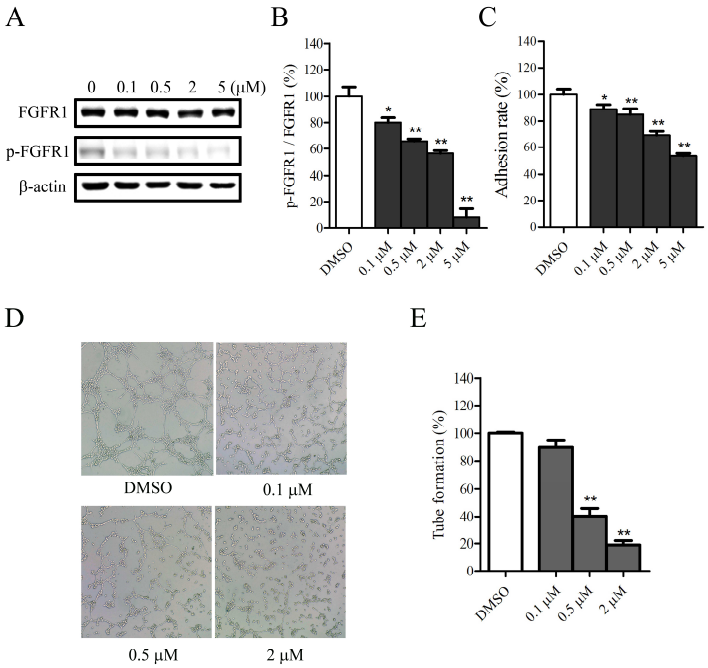

Fig. 5 Anti-angiogenesis effect of Compound **4i** on HUVEC cell line in a dose-dependent manner. A-B) Inhibition of FGFR1 phosphorylation. C) Adhesion assay of HUVEC treated with or without **4i**. D-E) Suppression of HUVEC tube formation. The images were collected randomly using the inverted microscope. The number of nodes was calculated by image J..Data were shown as Mean ± SD from three independent experiments. Data were mean ± SD, *n*=3. **P*<0.05, ***P*<0.01 *vs.* DMSO group.

3. Conclusions

In conclusion, we have synthesized a series of novel FGFR1 inhibitors. Molecular docking of the most potent inhibitor **4i** into binding site of FGFR1 was performed, and the results showed this compound could bind well in the FGFR1 active site. The present study revealed several features of the novel FGFR1 inhibitor **4i**, which has a strong inhibitory effect on the growth, angiogenesis and metastasis of GBM *in vitro* and *in vivo* through the blockade of the FGFR1 signaling pathway. Especially in an *in vivo* study, compound **4i** demonstrated proper pharmacokinetic profiles, toxicity, and higher efficacy against GBM in nude mouse models. This compound significantly reduced the rate of U-87MG cell migration and invasion, delayed cell cycle progression by stopping U-87MG cells in the G2/M phase and

showed a potent decrease of phosphorylation of FGFR1 and its downstream effectors Akt and Erk as well as nuclear factor-kappaB in a dose-dependent manner. Thus, compound **4i** might be a promising anti-angiogenic and anti-metastatic candidate for cancer therapy and merits further investigation.

4. Materials and Methods

4.1. Generary chemistry

All commercially available solvents and reagents were used without further purification. Thin-layer chromatography (TLC) was carried out on precoated silica gel plates (60 F254, 250 μm) and visualized with UV light. Column chromatography was performed using Silica gel 60 (40-63 μm). Melting points were determined on a Kofler apparatus as uncorrected values. ^{1}H NMR and ^{13}C NMR spectra were measured on Bruker Avance III 400 MHz spectrometer in DMSO-d_6 or $CDCl_3$ with chemical shift (δ) given in parts per million (ppm) relative to TMS as internal standard and recorded at 23°C. MS (ESI) was determined by using a API4000 QTRAP（AB SCIEX） spectrometer with TurboIonSpray source. High-resolution mass spectra (HRMS) were performed on Q Exactive Orbitrap ion trap (ESI, Thermo Scientific). The analyses of the final compounds indicated by the symbols of the elements performed in a EA-3000 apparatus（Eurovector，Italy）were within ± 0.4 % of the theoretical values.

*4.1.1. Synthesis of 2-amino-N-methylthiophene-3-carboxamide (**1a**)*

Triethylamine (12.83 g, 127 mmol) was added to a suspension of 1,4-dithiane-2,5-diol (9.73 g, 64 mmol) and 2-cyanoacetamide (6.27 g, 64 mmol) in ethanol (100 mL). The reaction mixture was heated at reflux for 1 h. The reaction mixture was cooled and filtered, and the filtrate was concentrated in vacuo. The crude mixture was dissolved in ethyl acetate (300 mL) and washed with 2.5 N aqueous sodium hydroxide solution (2 x 100 mL) and brine (3 x 100 mL). The organic layer was dried over magnesium sulfate, filtered and concentrated in vacuo to afford **1a** as yellow solid (7.99 g, 80%). ^{1}H NMR (400 MHz, DMSO-d_6) δ 7.64 (d, J = 4.4 Hz, 1H),

7.16 (s, 2H), 7.02 (d, *J* = 6.0 Hz, 1H), 6.26 (d, *J* = 6.0 Hz, 1H), 2.68 (d, *J* = 4.4 Hz, 3H). ^{13}C NMR (100 MHz, DMSO-d_6) δ166.4, 161.3, 124.5, 107.8, 106.2, 25.8. ESI-MS m/z: 157.1 $[M + H]^+$.

*4.1.2. General procedure for compounds **1b-d*** [34]

A mixture of cyanoacetamide (98 mg, 1 mol), sulfur (32 mg, 1 mol) and with triethylamine (303 mg, 3 mol) in EtOH (10 mL) was stirred at 45 °C. The resulting solution was treated dropwise with corresponding aldehyde (1 mol) over 1.5 h and maintained at 40-45 °C for overnight. It was cooled and poured onto water (60 mL) at 5 °C. The precipitate was collected by filtration, washed with water and dried. The solid obtained was recrystallized from propanol to give the above title compound.

2-amino-5-ethyl-N-methylthiophene-3-carboxamide (**1b**) Yellow solid; yield 64%; ^{1}H NMR (400 MHz, DMSO-d_6) δ 7.52 (d, *J* = 4.4 Hz, 1H), 7.00 (s, 2H), 6.71 (s, 1H), 2.65 (d, *J* = 4.4 Hz, 3H), 2.52 (q, *J* = 7.6 Hz, 2H), 1.15 (t, *J* = 7.6 Hz, 3H). ^{13}C NMR (100 MHz, DMSO-d_6) δ166.4, 159.6, 126.1, 119.8, 107.0, 25.8, 23.0, 15.8. ESI-MS m/z: 185.2 $[M + H]^+$.

2-amino-5-(tert-butyl)-N-methylthiophene-3-carboxamide (**1c**) Yellow solid; yield 66%; ^{1}H NMR (400 MHz, DMSO-d_6) δ 7.54 (d, *J* = 4.4 Hz, 1H), 6.97 (s, 2H), 6.75 (s, 1H), 2.66 (d, *J* = 4.4 Hz, 3H), 1.23 (s, 9H). ^{13}C NMR (100 MHz, DMSO-d_6) δ 166.5, 159.3, 135.9, 118.0, 106.8, 33.9, 32.2, 25.8. ESI-MS m/z: 213.4 $[M + H]^+$.

2-amino-N-methyl-5-phenylthiophene-3-carboxamide (**1d**) Yellow solid; yield 67%; ^{1}H NMR (400 MHz, DMSO-d_6) δ 7.74 (d, *J* = 4.4 Hz, 1H), 7.55 (s, 1H), 7.43 (s, 2H), 7.40 – 7.33 (m, 4H), 7.17 (t, *J* = 7.2 Hz, 1H), 2.72 (d, *J* = 4.4 Hz, 3H). ^{13}C NMR (100 MHz, DMSO-d_6) δ 166.3, 161.1, 134.7, 129.4, 126.3, 124.1, 122.0, 121.1, 108.8, 25.9. ESI-MS m/z: 233.1 $[M + H]^+$.

*4.1.3. Synthesis of 4-chloro-N-(4-morpholinophenyl)-5-(trifluoromethyl)pyrimidin-2-amine (**2a**)*

To a solution of 5-trifluoromethyl-2,4-dichloropyrimidine (432 mg, 2 mmol) in 1:1 DCE/t-BuOH (10/10 mL) was added zinc chloride (0.5 M solution in THF, 4.8

mL, 1.2 eq) at 0° C. After 1 hour, 4-morpholin-4-yl-phenylamine (356 mg, 2 mmol) was added and followed by the dropwise addition of a solution of triethylamine (222 mg, 2.2 mmol). After stirring for 4 hours, the reaction was concentrated. The crude was purified by silica-gel column using n-hexane/EtOAc = 2/1 to give **2a**. Yellow solid; yield 42%; ^{1}H NMR (400 MHz, DMSO-d_6) δ 10.44 (s, 1H), 8.72 (s, 1H), 7.51 (d, J = 8.0 Hz, 2H), 6.95 (d, J = 8.0 Hz, 2H), 3.74 (s, 4H), 3.08 (s, 4H). ^{13}C NMR (100 MHz, DMSO-d_6) δ 161.0, 158.5, 148.3, 130.6, 127.6, 124.9, 122.4, 115.8, 110.6, 66.5, 49.2. ESI-MS m/z: 359.2 $[M + H]^+$.

*4.1.4. General procedure for compounds **3a-d*** [35]

To a solution of 2-amino-thiophene-3-carboxylic acid methylamide (686 mg, 4.4 mmol) and $NaHCO_3$ (282 mg, 4.4 mmol) in anhydrous EtOH (5 mL) was added the corresponding dichloropyrimidine derivative (4 mmol) at room temperature. The resulted mixture was heated to reflux, stirred overnight and cooled to room temperature. The precipitate was filtered and washed with water to give the title compound.

Synthesis of 2-((2-chloro-5-(trifluoromethyl)pyrimidin-4-yl)amino)-N-methylthiophen e-3-carboxamide (**3a**) Yellow solid; yield 38%; ^{1}H NMR (400 MHz, DMSO-d_6) δ13.27 (s, 1H), 8.55 (br, 2H), 7.50 (d, J = 6.0 Hz, 1H), 7.15 (d, J = 6.0 Hz, 1H), 2.82 (d, J = 4.4 Hz, 3H). ^{13}C NMR (100 MHz, DMSO-d_6) δ 169.7, 166.2, 161.5, 156.3, 153.2, 146.0, 137.6, 131.4, 129.5, 126.3, 123.6, 122.8, 120.9, 117.4, 115.2, 66.6, 46.4, 42.2, 26.2. ESI-MS m/z: 337.5 $[M + H]^+$.

Synthesis of 2-((2,5-dichloropyrimidin-4-yl)amino)-N-methylthiophene-3-carboxami de (**3b**) Yellow solid; yield 42%; ^{1}H NMR (400 MHz, DMSO-d_6) δ13.27 (s, 1H), 8.55 (br, 2H), 7.50 (d, J = 6.0 Hz, 1H), 7.15 (d, J = 6.0 Hz, 1H), 2.82 (d, J = 4.4 Hz, 3H). ^{13}C NMR (100 MHz, DMSO-d_6) δ 166.1, 156.7, 155.77, 153.7, 145.3, 122.9, 118.3, 116.2, 114.7, 26.3. ESI-MS m/z: 302.1 $[M + H]^+$.

Synthesis of 2-((5-Bromo-2-chloropyrimidin-4-yl)amino)-N-methylthiophene-3-carbox amide (**3c**) Brown solid; yield 72%; ^{1}H NMR (400 MHz, DMSO-d_6) δ 13.26 (s, 1H), 8.54 (d, J = 5.8 Hz, 2H), 7.71 – 7.32 (m, 1H), 7.15 (d, J = 5.8 Hz, 1H), 2.82 (d, J =

4.5 Hz, 3H). ESI-MS m/z: 347.2 $[M + H]^+$.

Synthesis of 2-((2-Chloro-5-methylpyrimidin-4-yl)amino)-N-methylthiophene-3-carbo xamide (**3d**) White solid; yield 68%; ^{1}H NMR (400 MHz, DMSO-d_6) δ 12.73 (s, 1H), 8.47 (d, J = 4.4 Hz, 1H), 8.22 (s, 1H), 7.47 (d, J = 6.0 Hz, 1H), 7.06 (d, J = 6.0 Hz, 1H), 2.82 (d, J = 4.4 Hz, 3H), 2.20 (s, 3H). ESI-MS m/z: 283.2 $[M + H]^+$.

*4.1.5. General procedure for compounds **4a-d*** [35]

To a solution of compound **2a** (672 mg, 2 mmol) in TFE (2,2,2-trifluoroethanol, 8 mL) was added compound **1a-d** (2.4 mmol) and TFA (trifluoroacetic acid, 6 mmol). The resulted mixture was heated to reflux and stirred overnight. The mixture was cooled to room temperature, added with EtOAc (50 mL) and washed with saturated $NaHCO_3$ (50 mL). The organic layer was dried over magnesium sulfate, filtered and concentrated in vacuo. The crude was purified by silica-gel column using DCM/MeOH = 30/1 to afford the title compound.

Synthesis of N-methyl-2-((2-((4-morpholinophenyl)amino)-5-(trifluoromethyl)pyrimidi n-4-yl)amino)thiophene-3-carboxamide (**4a**) Yellow solid; yield 31%; mp: 230-231 °C. ^{1}H NMR (400 MHz, DMSO-d_6) δ 12.86 (s, 1H), 9.58 (s, 1H), 8.44 – 8.33 (m, 2H), 7.43 – 7.35 (m, 3H) 7.02 – 6.94 (m, 3H), 3.79 – 3.72 (m, 4H), 3.13 – 3.00 (m, 4H), 2.80 (d, J = 4.4 Hz, 3H). ^{13}C NMR (100 MHz, DMSO-d_6) δ 166.2, 156.3, 153.2, 146.1, 126.9, 126.8, 126.4, 123.8，123.7, 122.8, 117.3, 115.8, 115.2, 115.0, 66.6, 49.4, 26.2. HRMS：calcd for $C_{21}H_{21}F_3N_6O_2S$ $[M + H]^+$, 478.1399; found 478.1406. Anal. $C_{21}H_{21}F_3N_6O_2S$ (C, H, N, S).

Synthesis of 5-Ethyl-N-methyl-2-((2-((4-morpholinophenyl)amino)-5-(trifluoromethyl) pyrimidin-4-yl)amino)thiophene-3-carboxamide (**4b**) Yellow solid; yield 34%; mp: 252-253 °C. ^{1}H NMR (400 MHz, DMSO-d_6) δ 12.74 (s, 1H), 9.54 (s, 1H), 8.38 (s, 1H), 8.23 (s, 1H), 7.36 (s, 2H), 7.08 (s, 1H), 6.96 (d, J = 8.4 Hz, 2H), 3.75 (s, 4H), 3.10 (s, 4H), 2.76 (d, J = 4.4 Hz, 3H), 2.61 (s, 2H), 1.18 (s, 3H). ^{13}C NMR (100 MHz, DMSO-d_6) δ 166.3, 156.3, 153.0, 148.7, 146.0, 144.0, 137.1, 126.9, 126.4, 123.8, 118.4, 115.7, 115.5, 114.3, 66.6, 49.2, 26.2, 22.7, 16.1. HRMS：calcd for $C_{23}H_{25}F_3N_6O_2S$ $[M + H]^+$, 506.1712; found 506.1715. Anal. $C_{23}H_{25}F_3N_6O_2S$ (C, H, N,

S).

Synthesis of 5-(tert-butyl)-N-methyl-2-((2-((4-morpholinophenyl)amino)-5-(trifluoromethyl)pyrimidin-4-yl)amino)thiophene-3-carboxamide (**4c**) Yellow solid; yield 30%; mp: 295-296 °C. ^{1}H NMR (400 MHz, DMSO-d_6) δ 12.79 (s, 1H), 9.57 (s, 1H), 8.38 (s, 1H), 8.26 (s, 1H), 7.32 (s, 2H), 7.13 (s, 1H), 6.95 (d, *J* = 6.0 Hz, 2H), 3.75 (s, 4H), 3.09 (s, 4H), 2.76 (d, *J* = 4.4 Hz, 3H), 1.23 (s, 9H). ^{13}C NMR (100 MHz, DMSO-d_6) δ 165.3, 155.2, 152.1, 147.4, 145.7, 142.9, 129.4, 125.4, 125.1, 122.7, 115.5, 114.3, 114.2, 112.9, 65.6, 47.9, 33.2, 31.4, 25.1. HRMS：calcd for $C_{25}H_{29}F_3N_6O_2S$ $[M + H]^+$, 534.2025; found 534.2031. Anal. $C_{25}H_{29}F_3N_6O_2S$ (C, H, N, S).

Synthesis of N-methyl-2-((2-((4-morpholinophenyl)amino)-5-(trifluoromethyl)pyrimidin-4-yl)amino)-5-phenylthiophene-3-carboxamide (**4d**) Yellow solid; yield 38%; mp: 299-300 °C. ^{1}H NMR (400 MHz, DMSO-d_6) δ 12.90 (s, 1H), 9.70 (s, 1H), 8.44 (s, 2H), 7.84 (s, 1H), 7.43 – 7.28 (m, 6H), 6.96 (d, *J* = 6.0 Hz, 2H), 3.75 (s, 4H), 3.07 (s, 4H), 2.82 (d, *J* = 4.4 Hz, 3H). ^{13}C NMR (100 MHz, DMSO-d_6) δ 166.1, 156.5, 153.1, 148.9, 145.4, 141.1, 134.1, 131.1, 129.6, 129.1, 127.6, 126.4, 126.0, 125.0, 123.7, 119.0, 115.9, 115.5, 66.6, 49.2, 26.2. HRMS：calcd for $C_{27}H_{25}F_3N_6O_2S$ $[M + H]^+$, 554.1712, found 554.1719. Anal. $C_{27}H_{25}F_3N_6O_2S$ (C, H, N, S).

*4.1.6. General procedure for compounds **4e-p*** [35]

To a solution of compound **3** (1 mmol) in TFE (2,2,2-trifluoroethanol, 4 mL) was added the corresponding dichloropyrimidine derivative (1.2 mmol) and TFA (trifluoroacetic acid, 3 mmol). The resulted mixture was heated to reflux and stirred overnight. The mixture was cooled to room temperature, added with EtOAc (50 mL) and washed with saturated $NaHCO_3$ (50 mL). The organic layer was dried over magnesium sulfate, filtered and concentrated in vacuo. The crude was purified by silica-gel column using DCM/MeOH = 30/1 to afford the title compound.

Synthesis of N-methyl-2-((2-((3-morpholinophenyl)amino)-5-(trifluoromethyl)pyrimidin-4-yl)amino)thiophene-3-carboxamide (**4e**) Yellow solid; yield 41%; mp: 259-261 °C. ^{1}H NMR (400 MHz, DMSO-d_6) δ 12.92 (s, 1H), 9.65 (s, 1H), 8.48 (s, 1H), 8.41 (d, *J* = 4.4 Hz, 1H), 7.44 (d, *J* = 6.0 Hz, 1H), 7.26 (s, 1H), 7.21 – 7.17 (m, 2H), 7.00 (d, *J* =

5.2 Hz, 1H), 6.71 (d, *J* = 8.4 Hz, 1H), 3.77 – 3.67 (m, 4H), 3.14 – 3.04 (m, 4H), 2.80 (d, *J* = 4.4 Hz, 3H). ^{13}C NMR (100 MHz, DMSO-d_6) δ 166.2, 161.3, 156.3, 153.2, 151.7, 146.0, 139.9, 129.3, 126.3, 123.6, 122.9, 117.3, 115.2, 113.7, 111.1, 109.6, 66.6, 48.9, 26.2. HRMS：calcd for $C_{21}H_{21}F_3N_6O_2S$ $[M + H]^+$, 478.1399, found 478.1403. Anal. $C_{21}H_{21}F_3N_6O_2S$ (C, H, N, S).

Synthesis of 2-((2-((4-([1,4'-bipiperidin]-1'-yl)phenyl)amino)-5-(trifluoromethyl)pyrimidin-4-yl)amino)-N-methylthiophene-3-carboxamide (**4f**) Yellow solid; yield 34%; mp: 260-261 °C. ^{1}H NMR (400 MHz, DMSO-d_6) δ 12.86 (s, 1H), 9.54 (s, 1H), 8.41 (s, 2H), 7.50 – 7.35 (m, 3H), 6.96 – 6.92 (m, 3H), 2.79 (d, *J* = 4.4 Hz, 3H), 2.70 – 2.60 (m, 7H), 1.90 – 1.87 (m, 3H), 1.62 – 1.57 (m, 7H) 1.46 – 1.43 (m, 2H). ^{13}C NMR (100 MHz, DMSO-d_6) δ 166.2, 156.2, 153.2, 148.9, 148.0, 146.1, 127.9, 126.4, 123.7, 122.7, 117.3, 116.5, 116.2, 115.1, 50.0, 49.1, 48.5, 27.2, 26.2, 25.4, 24.0. HRMS：calcd for $C_{27}H_{32}F_3N_7OS$ $[M + H]^+$, 559.2341, found 559.2348. Anal. $C_{27}H_{32}F_3N_7OS$ (C, H, N, S).

Synthesis of 2-((2-((4-(4-(2-hydroxyethyl)piperazin-1-yl)phenyl)amino)-5-(trifluoromethyl)pyrimidin-4-yl)amino)-N-methylthiophene-3-carboxamide (**4g**) Yellow solid; yield 25%; mp: 182-183 °C. ^{1}H NMR (400 MHz, DMSO-d_6) δ 12.85 (s, 1H), 9.54 (s, 1H), 8.47 – 8.31 (m, 2H), 7.42 (br, 3H), 6.96 – 6.92 (m, 3H), 4.46 (s, 1H), 3.58 – 3.53 (m, 2H), 3.12 (s, 4H), 2.79 (d, *J* = 4.4 Hz, 3H), 2.61 (s, 4H), 2.49 – 2.41 (m, 2H). ^{13}C NMR (100 MHz, DMSO-d_6) δ 166.2, 156.3, 153.2, 148.4, 146.1, 130.8, 126.4, 123.7, 122.8, 122.5, 121.5, 117.3, 116.1, 115.0, 60.6, 58.9, 53.6, 49.1, 26.2. HRMS：calcd for $C_{23}H_{26}F_3N_7O_2S$ $[M + H]^+$, 521.1812, found 521.1819. Anal. $C_{23}H_{26}F_3N_7O_2S$ (C, H, N, S).

Synthesis of N-methyl-2-((2-((4-(2-morpholinoethoxy)phenyl)amino)-5-(trifluoromethyl)pyrimidin-4-yl)amino)thiophene-3-carboxamide (**4h**) Yellow solid; yield 40%; mp: 187-189 °C. ^{1}H NMR (400 MHz, DMSO-d_6) δ 12.88 (s, 1H), 9.62 (s, 1H), 8.47 – 8.30 (m, 2H), 7.63 – 7.36 (m, 3H), 6.96 – 6.93 (m, 3H), 4.10 – 4.08 (m, 2H), 3.67 – 3.51 (m, 4H), 2.79 (d, *J* = 4.4 Hz, 3H), 2.70 (s, 2H), 2.50 – 2.46 (m, 4H). ^{13}C NMR (100 MHz, DMSO-d_6) δ 166.2, 156.3, 155.5, 153.2, 146.8, 146.1, 132.1, 126.4, 123.7,

122.8, 117.3, 116.2, 115.1, 114.8, 66.6, 65.9, 57.5, 54.1, 26.2. HRMS：calcd for $C_{23}H_{25}F_3N_6O_3S$ $[M + H]^+$, 522.1661, found 522.1669. Anal. $C_{23}H_{25}F_3N_6O_3S$ (C, H, N, S).

Synthesis of N-methyl-2-((2-((4-(4-morpholinopiperidin-1-yl)phenyl)amino)-5-(trifluoromethyl)pyrimidin-4-yl)amino)thiophene-3-carboxamide (**4i**) Yellow solid; yield 34%; mp: 276-278 °C. ^{1}H NMR (400 MHz, DMSO-d_6) δ 12.85 (s, 1H), 9.52 (s, 1H), 8.47 – 8.29 (m, 2H), 7.54 – 7.24 (m, 3H), 7.00 – 6.92 (m, 3H), 3.70 (d, *J* = 11.6 Hz, 2H), 3.63 – 3.56 (m, 4H), 2.79 (d, *J* = 4.4 Hz, 3H), 2.67 (t, *J* = 11.6 Hz, 2H), 2.50 (s, 4H), 2.31 – 2.28 (m, 1H), 1.87 (d, *J* = 11.6 Hz, 2H), 1.54 – 1.44 (m, 2H). ^{13}C NMR (100 MHz, DMSO-d_6) δ 166.2, 156.3, 153.2, 150.2, 148.2, 146.2, 129.8, 126.4, 122.8，122.6, 117.4, 116.4, 115.7, 115.0, 66.4, 61.9, 49.7, 48.8, 27.5, 26.2. HRMS：calcd for $C_{26}H_{30}F_3N_7O_2S$ $[M + H]^+$, 561.2123, found 561.2126. Anal. $C_{26}H_{30}F_3N_7O_2S$ (C, H, N, S).

Synthesis of N-methyl-2-((2-((4-(2-morpholinoethyl)phenyl)amino)-5-(trifluoromethyl)pyrimidin-4-yl)amino)thiophene-3-carboxamide (**4j**) Yellow solid; yield 36%; mp: 250-251 °C. ^{1}H NMR (400 MHz, DMSO-d_6) δ 12.92 (s, 1H), 9.69 (s, 1H), 8.46 (s, 1H), 8.40 (d, *J* = 4.4 Hz, 1H), 7.55 (d, *J* = 6.4 Hz, 2H), 7.44 (d, *J* = 6.0 Hz, 1H), 7.20 (d, *J* = 8.4 Hz, 2H), 6.98 (s, 1H), 3.61 – 3.56 (m, 4H), 2.81 (d, *J* = 4.4 Hz, 3H), 2.75 – 2.69 (m, 2H), 2.56 – 2.53 (m, 2H), 2.45 (s, 4H). ^{13}C NMR (100 MHz, DMSO-d_6) δ 165.2, 160.3, 155.2, 152.2, 144.9, 136.1, 135.0, 128.0, 125.3, 122.6, 121.8, 119.9, 116.2, 114.1, 65.6, 59.6, 52.7, 31.3, 25.2. HRMS：calcd for $C_{23}H_{25}F_3N_6O_2S$ $[M + H]^+$, 506.1712, found 506.1715. Anal. $C_{23}H_{25}F_3N_6O_2S$ (C, H, N, S).

Synthesis of N-methyl-2-((2-((4-((morpholinosulfonyl)methyl)phenyl)amino)-5-(trifluoromethyl)pyrimidin-4-yl)amino)thiophene-3-carboxamide (**4k**) Yellow solid; yield 36%; mp: 276-278 °C; ^{1}H NMR (400 MHz, DMSO-d_6) δ 12.85 (s, 1H), 9.52 (s, 1H), 8.47 – 8.29 (m, 2H), 7.54 – 7.24 (m, 3H), 7.00 – 6.92 (m, 3H), 3.70 (d, *J* = 11.6 Hz, 2H), 3.63 – 3.56 (m, 4H), 2.79 (d, *J* = 4.4 Hz, 3H), 2.67 (t, *J* = 11.6 Hz, 2H), 2.50 (s, 4H), 2.31 – 2.28 (m, 1H), 1.87 (d, *J* = 11.6 Hz, 2H), 1.54 – 1.44 (m, 2H). ^{13}C NMR (100 MHz, DMSO-d_6) δ 166.2, 156.3, 153.2, 150.2, 148.2, 146.2, 129.8, 126.4,

122.8，122.6, 117.4, 116.4, 115.7, 115.0, 66.4, 61.9, 49.7, 48.8, 27.5, 26.2. HRMS：calcd for $C_{22}H_{23}F_3N_6O_4S_2$ $[M + H]^+$, 556.1174, found 556.1179. Anal. $C_{22}H_{23}F_3N_6O_4S_2$ (C, H, N, S).

Synthesis of 2-((2-((4-(2-(1,1-dioxidothiomorpholino)ethyl)phenyl)amino)-5-(trifluoro methyl)pyrimidin-4-yl)amino)-N-methylthiophene-3-carboxamide (**4l**) Yellow solid; yield 50%; mp: 220-221 °C. ^{1}H NMR (400 MHz, DMSO-d_6) δ 12.95 (s, 1H), 9.85 (s, 1H), 8.50 (s, 1H), 8.40 (d, *J* = 4.8 Hz, 1H), 7.67 (d, *J* = 7.2 Hz, 2H), 7.44 – 7.39 (m, 3H), 6.98 (d, *J* = 4.8 Hz, 1H), 4.43 (s, 2H), 3.61 – 3.57 (m, 4H), 3.15 – 3.10 (m, 4H), 2.80 (d, *J* = 4.4 Hz, 3H). ^{13}C NMR (100 MHz, DMSO-d_6) δ 166.2, 161.2, 156.3, 153.2, 145.9, 139.4, 131.5, 126.2, 124.5, 123.5, 122.8, 122.5, 117.4, 115.3, 66.4, 54.3, 46.1, 26.2. HRMS：calcd for $C_{22}H_{25}F_3N_6O_3S_2$ $[M + H]^+$, 554.1382, found 554.1387. Anal. calcd for $C_{22}H_{25}F_3N_6O_3S_2$ (C, H, N, S).

Synthesis of 2-((2-((2-methoxy-4-(4-morpholinopiperidin-1-yl)phenyl)amino)-5-(triflu oromethyl)pyrimidin-4-yl)amino)-N-methylthiophene-3-carboxamide (**4m**) White solid; 49% yield; mp: 166-167 °C; ^{1}H NMR (400 MHz, DMSO-d_6) δ 12.18 (s, 1H), 8.74 (s, 1H), 8.31 (d, *J* = 4.4 Hz, 1H), 7.97 (s, 1H), 7.50 (d, *J* = 8.7 Hz,2H), 7.41 (d, *J* = 5.9 Hz, 1H), 7.04 – 6.89 (m, 1H), 6.88 (d, *J* = 8.8 Hz,2H), 5.76 (s, 1H), 3.70 – 3.60 (m, 2H), 3.58 (s, 6H), 2.80 (d, *J* = 4.3 Hz, 3H), 2.59 (dd, *J* = 24.2, 12.7 Hz, 2H), 2.31 – 2.16 (m, 2H), 2.11 (s, 3H), 1.50 (dd, *J* = 20.5, 11.0 Hz, 4H). ^{13}C NMR (100 MHz, DMSO-d_6) δ 166.5, 156.1, 153.4, 150.3, 148.4, 146.2, 129.8, 126.4, 122.1，122.6, 116.4, 115.7, 115.0, 105.9, 98.2, 66.4, 61.9, 55.8, 49.7, 48.8, 27.5, 26.2. HRMS：calcd for $C_{27}H_{32}F_3N_7O_3S$ $[M + H]^+$, 591.2239, found 591.2244. Anal. $C_{27}H_{32}F_3N_7O_3S$ (C, H, N, S).

Synthesis of 2-((5-chloro-2-((4-(4-morpholinopiperidin-1-yl)phenyl)amino)pyrimidin-4-yl)amino)-N-methylthiophene-3-carboxamide (**4n**) Yellow solid; yield 40%; mp: 229-230 °C. ^{1}H NMR (400 MHz, DMSO-d_6) δ 12.65 (s, 1H), 9.18 (s, 1H), 8.38 (d, *J* = 4.4 Hz, 1H), 8.21 (s, 1H), 7.50 (d, *J* = 8.8 Hz, 2H), 7.43 (d, *J* = 6.0 Hz, 1H), 6.99 (d, *J* = 6.0 Hz, 1H), 6.92 (d, *J* = 8.8 Hz, 2H), 3.78 – 3.72 (m, 4H), 3.09 – 3.03 (m, 4H), 2.80 (d, *J* = 4.4 Hz, 3H). ^{13}C NMR (100 MHz, DMSO-d_6) δ 166.3, 158.5, 155.1, 152.7, 147.5, 146.5, 132.3, 122.9, 116.7, 116.1, 115.9, 114.7, 104.0, 66.6, 49.6, 26.2.

HRMS：calcd for $C_{25}H_{30}ClN_7O_2S$ [M + H]$^+$ 527.1820, found 527.1825. Anal. $C_{25}H_{30}ClN_7O_2S$ (C, H, N, S).

Synthesis of 2-((5-bromo-2-((4-(4-morpholinopiperidin-1-yl)phenyl)amino)pyrimidin -4-yl)amino)-N-methylthiophene-3-carboxamide (**4o**) White solid; yield 64%; mp: 247-248 ℃. ^{1}H NMR (400 MHz, DMSO-d_6) δ 12.58 (s, 1H), 9.14 (s, 1H), 8.37 (d, *J* = 4.4 Hz, 1H), 8.26 (s, 1H), 7.48 (t, *J* = 9.6 Hz, 2H), 7.43 (d, *J* = 5.9 Hz, 1H), 6.98 (d, *J* = 9.2 Hz, 2H), 6.94 (d, *J* = 8.7 Hz, 2H), 3.72 (d, *J* = 66.4 Hz, 4H), 2.80 (d, *J* = 4.4 Hz, 3H), 2.67 (dd, *J* = 21.8, 11.1 Hz, 4H), 2.08 (s, 4H), 1.59 (s, 4H). ^{13}C NMR (100 MHz, DMSO-d_6) δ 166.2, 157.5, 153.3, 150.4, 148.2, 146.4, 129.9, 126.6, 122.8, 116.4, 115.7, 115.0, 93.5, 66.4, 61.9, 49.7, 48.8, 27.5, 26.2. HRMS：calcd for $C_{25}H_{30}BrN_7O_2S$ [M + H]$^+$ 571.1365, 571.1369. Anal. $C_{25}H_{30}BrN_7O_2S$ (C, H, N, S).

Synthesis of N-methyl-2-((5-methyl-2-((4-(4-morpholinopiperidin-1-yl)phenyl)amino) pyrimidin-4-yl)amino)thiophene-3-carboxamide (**4p**) Yellow solid; yield 31%; mp: 241-242 ℃; ^{1}H NMR (400 MHz, DMSO-d_6) δ 12.18 (s, 1H), 8.74 (s, 1H), 8.31 (d, *J* = 4.4 Hz, 1H), 7.97 (s, 1H), 7.50 (d, *J* = 8.7 Hz, 2H), 7.41 (d, *J* = 5.9 Hz, 1H), 6.92 (d, *J* = 5.8 Hz, 1H), 6.91 – 6.74 (m, 2H), 5.76 (s, 1H), 3.64 (s, 2H), 3.58 (s, 6H), 2.80 (d, *J* = 4.3 Hz, 3H), 2.60 (t, *J* = 11.6 Hz, 2H), 2.25 (s, 2H), 1.86 (d, *J* = 11.1 Hz, 3H), 1.50 (d, *J* = 9.5 Hz, 4H). ^{13}C NMR (100 MHz, DMSO-d_6) δ 166.3, 156.4, 153.2, 150.4, 148.3, 146.1, 129.8, 126.4, 122.8, 117.4, 116.4, 115.7, 115.0, 66.4, 61.9, 49.7, 48.8, 27.5, 26.2, 14.3. HRMS：calcd for $C_{26}H_{33}N_7O_2S$ [M + H]$^+$, found 507.2419. Anal. $C_{26}H_{33}N_7O_2S$ (C, H, N, S).

4.2. Enzymetic inhibition activity in vitro

The inhibitory effect of compounds was determined by using ADP-Glo^{TM} FGFR1 Kinase Enzyme System (Catalog V9321, Promega, America). Briefly, the kinase reaction was carried out in the diluted buffer containing 40 mM Tri-HCl (pH 7.5), 20 mM $MgCl_2$, 0.1 mg/mL BSA and 50 μM DTT. Before the kinase reaction, different concentrations of compound and 6 ng/well FGFR1 kinase were added into white 384 well plates (Catalog 4512, Corning, America), followed by addition of 1 μg/well enzymetic substrate and 20 μM ATP. The plate was allowed to incubate at 30 ℃ for

60 min, then 5 μL ADP-Glo^{TM} reagent was added and followed by incubation for 40 min at 25 ℃. Finally, 10 μL of kinase detection reagent was added and allowed to incubate for 30 min at 25 ℃. The integral intensity of each well was recorded by luminescence modular of microplate reader (SpectraMax Paradigm, Molecular Devices, America), and the IC_{50} was calculated by Graphpad Prism v 5.0.

4.3. Molecular docking

Docking study was performed using Sybyl-X 2.0 software. The FGFR1 crystal structure (PDB ID 6c1c) was obtained from Protein Data Bank. The size of pocket and the degree of embedding in FGFR1 were evaluated by threshold and bloat parameters, which were determined as 0.65 and 1 respectively. Compound **4i** was built in sketch module and minimized in molecule module on SYBYL using the Tripos force field. H-bond was assumed when the distance between two electronegative atoms was less than 3.0 Å. Van der Waals interactions were considered in the range 3.0–4.0 Å. Then, the graphs were visualized with PyMOL Molecular Graphics System Version 2.5.

4.4. Cell culture

U-87 MG (Catalog TCHu138, National Collection of Authenticated Cell Cultures, China) cell line was cultured in DMEM (Catalog 11965092, Gibco, America) containing 10% fetal bovine serum (Catalog 16140071, Gibco, America) and 1% Penicillin-Streptomycin (Catalog 15140163, Gibco, America) at 37 ℃. HUVECs (Catalog CRL-1730, ATCC, America) were cultured in F12-K (Catalog 11765047, Gibco, America) with 10% fetal bovine serum, 0.03 mg/mL ECGS (Catalog CB-40006, Fisher Scientific, America) and 0.1 mg/mL (Catalog H3149, Sigma-Aldrich, China). When confluence reached 80%, cells were treated with 0.25% trypsin (Catalog 25200056, Gibco, America) and used at the passage number 4-10 for experiments.

4.5. Cell viability assay

3×10^3 Cells were seeded into 96 well plates, incubated for 24 h at 37 ℃ in an incubator with 5% CO_2 and treated with different concentration of compound in complete medium containing 0.5% DMSO. After 48 h, the culture was replaced with 0.5 mg/mL 3-(4,5)-dimethylthiahiazo(-2)-3,5-diphenytetrazoliumromide (MTT, Catalog M2003, Merck, China) in serum-free medium, then incubated for 4 h. Finally, MTT solution was removed and 200 μL of DMSO was added to solubilize the formazan precipitate, and the absorbance was measured at 570 nm.

4.6. ADMET and pharmacokinetic studies

For ADMET studies, compound **4i** was built and full minimized using CHARMM force field using Discovery Studio 2.5 software (Accelrys, Inc., San Diego, Calif.). The low-energy conformers were used to calculate the ADMET properties.

For pharmacokinetic study, compound **4i** was dispersed in sodium carboxymethyl cellulose and administered orally at dose of 52.5 mg/kg per rats (n=5). Following oral administration, the blood (0.2 mL) was collected in citrate sodium treated microcentrifuge tubes at 0, 0.08, 0.5, 1, 2, 4, 6, 8, 10, 12, 24, 48 h. The plasma sample (75 μL) was collected by centrifuged at 1200×g for 10 min and deproteinated with acetonitrile at 16,000 g for 15 min at 4 ℃. The concentration of **4i** in plasma was analyzed using ultra high pressure liquid chromatography (Shimadzu, Japan) with C18 chromatographic column at a flow rate of 0.8 mL/min. The elution buffer was consisted of 83% methanol and 17% containing 0.1% formic acid.

4.7. Tumor xenograft

Tumor cells (1×10^7) were subcutaneously injected into six weeks old nude mice (20 ± 2g). After the tumor volume was developed into about 100 mm^3, mice were randomly assigned into vehicle (0.5 % methylcellulose) or treated groups (50 or 75 mg/kg/d of compound **4i** in 0.5 % methylcellulose), which were administered orally at five times a week for 4 week. The tumor volume and mice weight were monitored three times per week. Mice were sacrificed after 28 days and the tumor tissues were collected for next experiments. All of the animal experiment progress was performed

according to the guideline of Institutional Animal Care and Use Committee.

4.8. Western Blotting

HUVEC or U-87 MG cells were seeded into 6 well plates and incubated at 37 ℃ in an incubator with 5% CO_2 for 24 h. The medium was replaced with different concentrations of compound **4i**, then allowed to incubate for 48 h. To prepare the lysis, cells or tumor tissue were washed with cold PBS, lysed in the lysis buffer (Catalog P0013B, Beyotime Biotechnology, China) containing 50 mM Tris (pH 7.4), 150 mM NaCl, 1% Triton X-100, 1% sodium deoxycholate, 0.1% SDS, protease inhibitor and phosphatase inhibitor (Catelog P1045, Beyotime Biotechnology, China) for 20 min and collected by centrifugation at 10000×g for 5 min at 4 ℃. The protein quantitation of each supernatant was assessed by BCA Protein Assay Kit (Catalog P0011, Beyotime Biotechnology, China). Western Blotting was then performed as previouly described [35]. The primary antibodies used were following: FGFR1 (1:1500, Catalog AF6165 , Affinity Biosciences LTD., China), or p-FGFR1 (Tyr654, 1:1500, Catalog AF3157, Affinity Biosciences LTD., China), or pan-Akt (1:1000, Catalog 4691T, or Cell Signaling Technology, America), or p-Akt1 (1:1000, Catalog 9018T, Cell Signaling Technology, America), or Erk1/2 (1:1000, Catalog 4695T, Cell Signaling Technology, America), or p-Erk1/2 (1:1500, Catalog 4370T, Cell Signaling Technology, America), or NF-κB (1:5000, Catalog ab32536, ABcam, England), p-NF-κB (1:1000, Catalog ab76302, ABcam, England), or MMP-2 (1:3000, Catalog ab92536, ABcam, England), or MMP-9 (1:5000, Catalog ab76003, ABcam, England) or β-actin (1:10000, Catalog AF7018, Affinity Biosciences LTD., China).

4.9. Immunohistochemistry

Tumor tissues were fixed with 4% paraformaldehyde at 4 ℃ overnight and paraffin-embedded. The 4 μm sections underwent antigen retrieval, endogenous peroxidase blocking. After washing with PBS three times, all sections were treated for 12 h with primary antibody : MMP-2 (Catalog ab97779, ABcam, England), MMP-9 (Catalog ab76003, ABcam, England), Ki67 (GB111499, Wuhan Service

Biotechnology Co., Ltd) and CD31 (GB113151, Wuhan Service Biotechnology Co., Ltd) and then with the second antibody (Catalog AB-0041, Beijing Dingguo Changsheng Biotechnology CO. LTD, China) for 30 min. The sections were finally incubated with SABC-HRP kit (Catalog P0603, Beyotime Biotechnology, China) at 37 ℃ for 30 min, washed with PBS three times, stained with DAB and counterstained with hematoxylin. Images were collected on the Olympus IX71 inverted microscope and analysis with Image J.

4.10. Cell cycle analysis

Cell cycle profiles of U-87MG cells were determined by using propidium iodide (PI) staining kit (Catalog C1052, Beyotime Biotechnology, China). Briefly, cells (2×10^5/well) were plated into 6-well cell culture plates and followed by incubation for 24 h. The medium was then substituted with fresh culture medium containing different concentrations of compound. After incubation for 48 h, cells were resuspended, washed with PBS twice and centrifuged at 800×g for 5 min. Pre-colded 70% ethanol was used to fix the cells for 36 h at -20 ℃. Before staining with the mixture of PI and RNAase for 20 min at 37 ℃, cells were washed twice with PBS. The Flowsight flow cytometer (Merck, America) was used to detect the fluorescence intensity of each cell.

4.11. Wound healing assay

U-87 MG cells were plated into 6 well plates, incubated to complete confluence, scratched with 10 μL pipette tips and washed four times with PBS. Cells were treated with 0.1% DMSO or difference concentration of compound **4i** in culture containing 1% FBS for 24 h. Images of cells were captured at 0 h and 24 h by using JuLI-B004 cell monitor (NanoEntek, Korea). The width of wound was marked and analyzed with image J.

4.12. Invasion assay

The top chamber of Transwell 24 well plates (Catalog 354234, Corning, America)

were used to pre-coat the 1:9 dilution Matrigel with serum-free DMEM at 25 ℃ for 24 h. U-87 MG cells were pre-treated with 0.1% DMSO or compound **4i** (0.3 or 3 μM) for 20 min and plated into Matrigel pre-coated top chamber at a density of 1×10^4 cells/well (100 μL/well). 600 μL of complete medium was added into the bottom chamber of the plate. Cells were allowed to shift through the Matrigel pre-coated membrane for 24 h. The cells that were not transferred under the membrane were removed with cotton stick, washed with PBS three times, fixed with 4% paraformaldehyde for 30 min and stained with 0.1% crystal violet for 30 min. After staining, the top chamber was washed again with PBS three times and migrated cells were imaged (×100) randomly in six areas by inverted microscope (Olympus IX71, Japan). The number of cells in each image was counted by image J.

4.13. Tube formation assay

Thawed Matrigel (50 μL/well) was added to 96 well plates on the ice and followed by 30 min incubation at 37 ℃. HUVECs were suspended and incubated in complete medium containing 0.1% DMSO or compound **4i** at 0.1, 0.5 and 2 μM for 30 min. The cells were added into the wells coated with Matrigel and the plates were placed at 37 ℃ with 5% CO_2 for 6 h. Then, tube formation was imaged using an inverted microscope (Olympus IX71, Japan).

4.14. Statistical analysis

All the experiments data were presented as mean ± standard deviation (SD) or mean ± standard error of mean (SEM), and analyzed by using GraphPad Prism v5. Differences between two groups were analyzed by one way ANOVA and considered significant when $p < 0.05$.

Declaration of competing interest

The authors declare no potential conflicts of interest.

Acknowledgements

This work was funded by the National Natural Science Foundation of China (Grants 21672043 and 22178070).

Appendix A. Supplementary data

Supplementary data to this article can be found online at

References

[1] L.R. Schaff, I.K. Mellinghoff, Glioblastoma and Other Primary Brain Malignancies in Adults: A Review, JAMA. 329 (2023) 574–587, https://doi.org/10.1001/jama.2023.0023.

[2] F.H. Al-Ostoot, S. Salah, H.A. Khamees, S.A. Khanum. Tumor angiogenesis: Current challenges and therapeutic opportunities, Cancer Treat Res Commun. 28 (2021) 100422, https://doi.org/10.1016/j.ctarc.2021.100422.

[3] S.A. Patel, M.B. Nilsson, X. Le, T. Cascone, R.K. Jain, J.V. Heymach, Molecular Mechanisms and Future Implications of VEGF/VEGFR in Cancer Therapy, Clin Cancer Res. 29 (2023) 30–39, https://doi.org/10.1158/1078-0432.ccr-22-1366.

[4] B.K. Ahir, H.H. Engelhard, S.S. Lakka, Tumor Development and Angiogenesis in Adult Brain Tumor: Glioblastoma, Mol. Neurobiol. 57 (2020) 2461–2478, https://doi.org/10.1007/s12035-020-01892-8.

[5] T.T. Batchelor, D.G. Duda, E.D. Tomaso, M. Ancukiewicz, S.R. Plotkin, E. Gerstner, A.F. Eichler, J. Drappatz, F.H. Hochberg, T. Benner, D.N. Louis, K.S. Cohen, H. Chea, A. Exarhopoulos, J.S. Loeffler, M.A. Moses, P. Ivy, A.G. Sorensen, P.Y. Wen, R.K. Jain, Phase II study of cediranib, an oral pan-vascular endothelial growth factor receptor tyrosine kinase inhibitor, in patients with recurrent glioblastoma, J. Clin. Oncol. 28 (2010) 2817–2823, https://doi.org/10.1200/JCO.2009.26.3988.

[6] A. Qin, A. Musket, P.R. Musich, J.B. Schweitzer, Q. Xie, Receptor tyrosine kinases as druggable targets in glioblastoma: Do signaling pathways matter?, Neurooncol Adv. 3 (2021) vdab133, https://doi.org/10.1093/noajnl/vdab133.

[7] Y. Itatani, K. Kawada, T. Yamamoto, Y. Sakai, Resistance to Anti-Angiogenic Therapy in Cancer-Alterations to Anti-VEGF Pathway, Int J Mol Sci. 19 (2018) 1232, https://doi.org/10.3390/ijms19041232.

[8] G. Bergers, D. Hanahan, Modes of resistance to anti-angiogenic therapy, Nat. Rev. Cancer 8 (2008) 592–603, https://doi.org/10.1038/nrc2442.

[9] M. Pàez-Ribes, E. Allen, J. Hudock, T. Takeda, H. Okuyama, F. Viñals, M. Inoue, G. Bergers, D. Hanahan, O. Casanovas, Antiangiogenic Therapy Elicits Malignant Progression of Tumors to Increased Local Invasion and Distant Metastasis, Cancer Cell 15 (2009) 220–231, https://doi.org/10.1016/j.ccr.2009.01.027.

[10] J. Jászai, M.H.H. Schmidt, Trends and Challenges in Tumor Anti-Angiogenic Therapies, Cells 8 (2019) 1102, https://doi.org/10.3390/cells8091102.

[11] X. Jiang, Y. Huang, X. Wang, Q. Liang, Y. Li, F. Li, X. Fu, C. Huang, H. Liu, Dianhydrogalactitol, a potential multitarget agent, inhibits glioblastoma migration, invasion, and angiogenesis, Biomed Pharmacother 91 (2017) 1065–1074, https://doi.org/10.1016/j.biopha.2017.05.025.

[12] Z. Chen, L.J. Tong, B.Y. Tang, H.Y. Liu, X. Wang, T. Zhang, X.W. Cao, Y. Chen, H.L. Li, X.H. Qian, Y.F. Xu, H. Xie, J. Ding, C11, a novel fibroblast growth factor receptor 1 (FGFR1) inhibitor, suppresses breast cancer metastasis and angiogenesis, Acta Pharmacol Sin. 40 (2019) 823–832, https://doi.org/10.1038/s41401-018-0191-7.

[13] V. Rand, J. Huang, T. Stockwell, S. Ferriera, O. Buzko, S. Levy, D. Busam, K. Li, J.B. Edwards, C. Eberhart, K.M. Murphy, A. Tsiamouri, K. Beeson, A.J.G Simpson, J.C. Venter, G.J. Riggins, R.L. Strausberg, Sequence survey of receptor tyrosine kinases reveals mutations in glioblastomas, Proc. Natl. Acad. Sci. U. S. A. 102 (2005) v14344–14349, https://doi.org/10.1073/pnas.0507200102.

[14] M. Katoh, H. Nakagama, FGF receptors: cancer biology and therapeutics, Med. Res. Rev. 34 (2014) 280–300, https://doi.org/10.1002/med.21288.

[15] A. Kowalski-Chauvel, V. Gouaze-Andersson, L. Baricault, E. Martin, C. Delmas, C. Toulas, E. Cohen-Jonathan-Moyal, C. Seva, Alpha6-integrin regulates FGFR1 expression through the ZEB1/YAP11/transcription complex in glioblastoma stem cells resulting in enhanced proliferation and stemness, Cancers (Basel) 11 (2019) 406, https://doi.org/10.3390/cancers11030406.

[16] R.S. Morrison, F. Yamaguchi, J.M. Bruner, M. Tang, W. McKeehan, M.S. Berger, Fibroblast Growth Factor Receptor Gene Expression and Immunoreactivity Are Elevated

in Human Glioblastoma Multiforme, Cancer Res. 54 (1994) 2794–2799.

[17] R.S. Morrison, F. Yamaguchi, H. Saya, J.M. Bruner, A.M. Yahanda, L.A. Donehower, M. Berger, Basic fibroblast growth factor and fibroblast growth factor receptor I are implicated in the growth of human astrocytomas, J. Neurooncol. 18 (1994) 207–216, https://doi.org/10.1007/BF01328955.

[18] J. Fukai, H. Yokote, R. Yamanaka, T. Arao, K. Nishio, T. Itakura, EphA4 promotes cell proliferation and migration through a novel EphA4-FGFR1 signaling pathway in the human glioma U251 cell line, Mol. Cancer Ther. 7 (2008) 2768–2778, https://doi.org/10.1158/1535-7163.MCT-07-2263.

[19] S. Miyamoto, S. Kakutani, Y. Sato, A. Hanashi, Y. Kinoshita, A. Ishikawa, Drug review: Pazopanib, Jpn J Clin Oncol. 48 (2018) 503-513, https://doi.org/10.1093/jjco/hyy053.

[20] A. Grothey, J.Y. Blay, N. Pavlakis, T. Yoshino, J. Bruix, Evolving role of regorafenib for the treatment of advanced cancers, Cancer Treat Rev. 86 (2020) 101993, https://doi.org/10.1016/j.ctrv.2020.101993.

[21] Y. Zhao, Y.N.Zhang, K.T. Wang, L. Chen, Lenvatinib for hepatocellular carcinoma: From preclinical mechanisms to anti-cancer therapy, Biochim Biophys Acta Rev Cancer. 1874 (2020) 188391, https://doi.org/10.1016/j.bbcan.2020.188391.

[22] A. Franza, M. Pirovano, P. Giannatempo, L. Cosmai, Erdafitinib in locally advanced/metastatic urothelial carcinoma with certain FGFR genetic alterations, Future Oncol. 18 (2022) 2455–2464, https://doi.org/10.1016/j.bbcan.2020.188391.

[23] S. Sadeghi, Infigratinib for cholangiocarcinoma, Drugs Today (Barc). 58 (2022) 327–334, https://doi.org/10.1358/dot.2022.58.7.3408813.

[24] A. Rizzo, A.D. Ricci, G. Brandi, Pemigatinib: Hot topics behind the first approval of a targeted therapy in cholangiocarcinoma, Cancer Treat Res Commun. 27 (2021) 100337, https://doi.org/10.1016/j.ctarc.2021.100337.

[25] W. Zhou, A. Huang, Y. Zhang, Q. Lin, W. Guo, Z. You, Z. Yi, M. Liu, Y. Chen, Design and optimization of hybrid of 2,4-diaminopyrimidine and arylthiazole scaffold as anticancer cell proliferation and migration agents, Eur J Med Chem. 96 (2015) 269–280, https://doi.org/10.1016/j.ejmech.2015.04.027.

[26] S. Sawayama, R. Murakami, M. Aki, Y. Kawaguchi, Y. Takao, H. Nonogaki, T. Goto, C.

Yamauchi, Efficacy of pazopanib in FGFR1-amplified uterine carcinosarcoma: A case report, Gynecol Oncol Rep. 41 (2022) 100993, https://doi.org/10.1016/j.gore.2022.100993.

[27] A.N. Jain, Scoring noncovalent protein-ligand interactions: a continuous differentiable function tuned to compute binding affinities, J Comput Aided Mol Des. 10 (1996) 427–440, https://doi.org/10.1007/bf00124474.

[28] H. Cho, N. Kim, T. Murakami, T. Sim, Anti-Tumor Activity of AZD4547 Against NTRK1 Fusion Positive Cancer Cells Through Inhibition of NTRKs, Front Oncol. 11 (2021) 757598, https://doi.org/10.3389/fonc.2021.757598.

[29] M. Wang, T. Wang, S. Liu, D. Yoshida, A. Teramoto, The expression of matrix metalloproteinase-2 and -9 in human gliomas of different pathological grades, Brain Tumor Pathol. 20 (2003) 65-72, https://doi.org/10.1007/bf02483449.

[30] G.A. Conlon, G.I. Murray, Recent advances in understanding the roles of matrix metalloproteinases in tumour invasion and metastasis, J Pathol. 247 (2019) 629-640, https://doi.org/10.1002/path.5225.

[31] J.H. Uhm, N.P. Dooley, J.G. Villemure, V.W. Yong, Mechanisms of glioma invasion: role of matrix-metalloproteinases, Can. J. Neurol. Sci. 24 (1997) 3–15, https://doi.org/10.1017/s0317167100021028.

[32] J. Fang, Y. Shing, D. Wiederschain, L. Yan, C. Butterfield, G. Jackson, J. Harper, G. Tamvakopoulos, M.A. Moses, Matrix metalloproteinase-2 is required for the switch to the angiogenic phenotype in a tumor model, Proc. Natl. Acad. Sci. U. S. A. 97 (2000) 3884–3889, https://doi.org/10.1073/pnas.97.8.3884.

[33] A. Vollmann-Zwerenz, V. Leidgens , G. Feliciello, C.A. Klein, P. Hau, Tumor Cell Invasion in Glioblastoma, Int J Mol Sci. 21 (2020) 1932, https://doi.org/10.3390/ijms21061932.

[34] K. Wang, D. Kim, A. Do¨mling. Cyanoacetamide MCR (III): Three-Component Gewald Reactions Revisited, J. Comb. Chem. 12(2010) 111–118, https://doi.org/10.1021/cc9001586.

[35] B. Li, Y. Li, C. Tomkiewicz-Raulet, P. Dao, D. Lietha, E. Yen-Pon, Z. Du, X. Coumoul, C. Garbay, M. Etheve-Quelquejeu, H. Chen, Design, synthesis and biological evaluations of covalent inhibitors of Focal Adhesion Kinase (FAK) against human malignant glioblastoma, J. Med. Chem. 63 (2020) 12707–12724,

https://doi.org/10.3390/ijms21061932.

Design, synthesis and evaluation of novel pyrimidinylaminothiophene derivatives as FGFR1 inhibitors against human glioblastoma multiforme

Yongliang Li, Long-Jia Yan, Hui-Xiong Chen, Ban-Kang Ruan, Pascal Dao, Zhi-Yun Du, Chang-Zhi Dong, Bernard Meunier

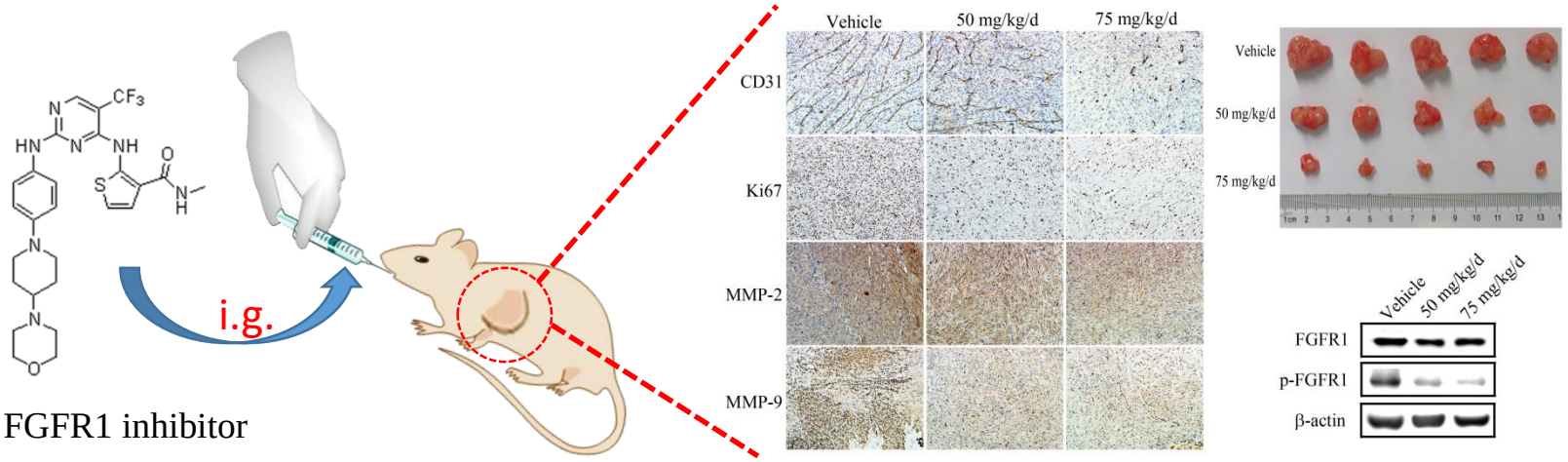

4i : FGFR1 inhibitor